ARCHIVES

Scanned Pulsed Laser Annealing of Cu Thin Films

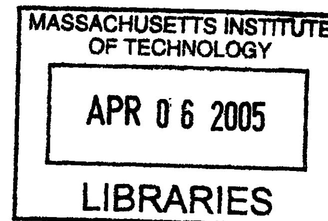

by

Harsh Anand Verma

B.Tech., Metallurgical Engineering

Indian Institute of Technology, Madras, 2001

Submitted to the Department of Materials Science and Engineering
in partial fulfillment of the requirements for the degree of

Master of Science

at the

Massachusetts Institute of Technology

September 2004

© 2004 Massachusetts Institute of Technology
All rights reserved

Signature of Author..
Department of Materials Science and Engineering
August 27, 2004

Certified by..
Carl V. Thompson
Stavros Salapatas Professor of Materials Science and Engineering
Thesis Supervisor

Accepted by..
Carl V. Thompson
Stavros Salapatas Professor of Materials Science and Engineering
Chairman, Departmental Committee on Graduate Students

Scanned Pulsed Laser Annealing of Cu Thin Films

by

Harsh Anand Verma

Submitted to the Department of Materials Science and Engineering
on Aug 27th, 2004 in partial fulfillment of the requirements for the degree of
Master of Science in Electronic, Photonic and Magnetic Materials

Abstract

As the microelectronics industry has moved to Cu as the conductor material, there has been much research into microstructure control in Cu thin films, primarily because grain sizes affect resistivity. Also with Cu-based interconnects, interfacial electromigration is the dominant mechanism, and therefore the crystallographic orientation of the grains could influence reliability. Scanned laser annealing can, in principle, be used to develop test structures with extremely large grains which could be used to quantify the effects of grain boundary scattering and the role of crystallographic orientation in interfacial electromigration.

Earlier research on scanned continuous laser annealing suggested that control of the thermal gradient would lead to an improved ability to manipulate grain structures. A scheme to alter the thermal profile during scanned pulsed laser annealing is implemented in the present work. Annealing of samples with Cu thin films over Si substrates with and without a silicon dioxide layer were investigated.

Samples were scanned at three different velocities over a range of powers. Ablation was observed at high powers. Quasi-periodic agglomerated structures were observed below threshold powers for ablation, and grain growth was observed at lower powers. The powers at which these regimes occur, shifted towards lower power for the sample with an oxide layer. The period of the agglomerated structures was found to decrease as the power was increased and as the velocity was decreased.

To clarify the effects of thermal gradient, thermal analysis based on finite element modeling was done to identify equivalent annealing conditions for the two kinds of samples. Scaling equations to account for the affect of power and pulsing frequency on temperatures and cooling times in the sample with an oxide layer were formulated. Under equivalent conditions, the average grain length in the scanning direction was found to be higher in the sample without an oxide layer. The average grain lengths in the direction perpendicular to the scanning direction were found to be comparable. This supports expectations based on earlier work.

Thesis Supervisor: Carl V. Thompson
Title: Stavros Salapatas Professor of Materials Science and Engineering

ACKNOWLEDGEMENTS

I am very grateful for the advice and support of my advisor, Prof. Carl V. Thompson, for his feedback and for keeping me focused in my research.

I thank all the members of my research group for being very tolerant and helpful to me. I would like to mention Rajappa, Andrew and Rob for their help and assistance.

Special thanks to all the staff at CMSE, MTL, and Harvard CIMS. Jung Choe and Kathy Farrell were really helpful and took care of the administrative details and I am immensely thankful to them.

I also thank my friends and family members for their constant encouragement and support.

Contents

LIST OF FIGURES 6

LIST OF TABLES 9

1 INTRODUCTION 10

1.1 Laser Processing 10

1.2 Microstructure Evolution using Scanned Laser Beam 11

1.2.1 Grain growth in thin films 12

1.2.2 Grain growth in presence of moving heat zone 12

1.3 Motivation for Present Work 17

2 EXPERIMENTS 20

2.1 Laser Set-up 20

2.2 Samples 21

2.3 Laser Scanning and Analysis 22

3 THERMAL MODELING 24

3.1 Introduction 25

3.2 Results 26

3.3 Equivalent conditions to study the effect of thermal gradient on grain growth 28

3.3(a) Scaling of Power 28

3.3(b) Scaling of Pulsing frequency 29

3.3(b).1. Introduction 29

3.3(b).2. MATLAB simulations for grain growth and thermal dose 30

4 RESULTS AND DISCUSSION 33

4.1 Regimes 33

4.2 Ablation 34

4.3 Agglomeration 36

4.2 Grain Growth 37

4.2.1 Effect of power and scanning velocity 38

4.2.2 Effect of thermal gradient 40

5 SUMMARY AND FUTURE WORK 48

5.1 Summary 48

5.2 Future Work 49

BIBLIOGRAPHY 51

List of Figures

1-1	Microstructural map of the microstructure regimes defined by laser power and scan velocity for Al. The final microstructure are agglomerated(X), bamboo (B), and polygranular (P).	13
1-2	Microstructural map of the microstructure regimes defined by laser power and scan velocity for Cu. The final microstructure are agglomerated(X), bamboo (B), and polygranular (P).	14
1-3	Plot of dependence of the average bamboo grain length as a function of laser power and scan rate for fully bamboo structures in Al.	15
1-4	Plot of dependence of the average bamboo grain length as a function of laser power and scan rate for fully bamboo structures in Cu.	16
1-5	Various microstructure regimes depending on scanning velocity (Simulations).	16
1-6	Grain growth simulation showing that a steeper thermal gradient, or a smaller Γ, leads to longer bamboo grain lengths.	17
1-7	Resistivity increase as the line width decrease (FS model accounts for the surface scattering as size goes down, and MS model accounts for the grain boundary scattering).	18
2-1	Schematic diagram of scanned laser annealing setup.	20
2-2	(a) Sample without the oxide layer (b) Sample with the oxide layer.	21
3-1	Geometry for FEM analysis: Cylinder 30μm radius, 50 μm height axis	25

symmetric element with z axis as the axis of rotation.

3-2 (a) Cooling curve at the center of the beam for sample with no oxide layer. 26

3-2 (b) Cooling curve at the center of the beam for sample with an oxide layer 27

3-3 Cooling curves after adjusting powers (Power in sample with oxide scaled down). 29

3-4 Comparison of the cooling curves after scaling of powers. 30

3-5 Thermal gradients in the scanning direction. 32

4-1 (a) Regimes of Scanned laser annealing for sample without any oxide layer. 33

4-1 (b) Regimes of Scanned laser annealing for sample with an oxide layer. 34

4-2 Images of ablated region (a) at P = 1.9W, v = 1 μm/s, sample with an oxide layer (b) at P = 2.8 W, v = 1 μm/s, sample without an oxide layer. 35

4-3 (a) Agglomerated structures over different power and velocities for the sample without an oxide layer. 36

4-3 (b) Agglomerated structures over different power and velocities for the sample with an oxide layer. 37

4-4 (a) Grain growth over different power and velocities for the sample without an oxide layer. 38

4-4 (b) Grain Growth over different power and velocities for the sample with an oxide layer. 39

4-5 (a) and (b) Comparison between grain growths at equivalent points in the two samples for scanning velocity of 1 μm/s. 41

4-6 Comparison between grain growths at equivalent points in the two 42

samples for scanning velocity of 5 μm/s.

4-7 (a) and (b) Comparison between grain growths at equivalent points in the two samples for scanning velocity of 60 μm/s. 43

4-8 Average grain size in the scanning direction under three conditions. 44

4-9 Average grain size in the direction perpendicular to the scanning direction under three conditions. 45

4-10 Average ratio of the grain length in the scanning direction to the grain length in the perpendicular direction. 45

4-11 Thermal gradients in the scanning direction for conditions 1 and 2. 46

4-12 Thermal gradients in the scanning direction for condition 3. 47

List of Tables

Table 3-1 Material properties used in FEM analysis. 24

Table 4-1 Ratio of maximum temperature attained at the ablation threshold for the sample with oxide layer and the sample with no oxide layer at different velocities. 35

CHAPTER 1

Introduction

1.1 Laser processing

The unique property of laser beams to be able to deliver energy with extreme spatial and temporal control has made them useful for many applications in materials processing. The range of applications in materials processing encompasses surface modification [Ohr92], welding [Dar85], cutting and trimming [Hil00], repair of structures such as interconnects [Ras96, She96], photolithography, film deposition [Ohr92] and several other applications [Maz04, Ven04].

Both continuous wave (CW) and pulsed lasers are used for material processing. CW laser have advantages such as better control in terms of output power and stability compared to pulsed laser. However, using a pulsed laser a significant amount of energy can be delivered into a substrate, before heat can diffuse much during the irradiation time of the pulse. Therefore, less energy is required to heat the sample to the desired temperature, and the rest of the substrate is subjected to minimal heating. The deposition of energy in very short time leads to rapid heating and quenching due to which novel microstructures can be formed. Meta-stable phases which are not formed by conventional annealing can be formed using pulsed laser processing [Urb02]. On the other hand, CW lasers are used for applications where larger dwell times are required such as laser surface alloying, where it leads to complete homogenization [Ohr92].

There are two characteristic time constants which decide how the laser energy is absorbed in the material: the electron-phonon relaxation time τ_e and the auger relaxation

time τ_A. The typical value of τ_e is of the order of 1ps and τ_A is of the order of 1-10ps[Lom84]. Pulsed laser processing using lasers which have pulse duration of nanosecond or longer, which is more than the characteristic time constants, is considered to be purely thermal process. Processes using ultra-short pulses such as femto-second laser processing are modeled by non-equilibrium mechanisms [Iti04].

In micro-electronics industry, laser processing was studied for annealing of ion-implanted layer[Nar83].Crystallization of amorphous silicon by laser annealing was also extensively researched[Yog93].Lasers are now used in deposition of thin films by Laser assisted Chemical Vapor Deposition(LCVD) and by pulsed laser deposition(PLD). Lasers are also used for applications including direct writing using laser mask projection[Gow99], production of micro-electromechanical devices(MEMS) by laser machining[Rum96] and repair of integrated circuits chip for yield enhancement[Ber95].

1.2 Microstructure Evolution using Scanned laser beam

1.2.1 Grain growth in thin films

Grain growth in thin films can occur during deposition or post deposition.
For bulk three dimensional systems the grain growth is found to follow the laws of normal grain growth and it obeys the following equation [Tho90]

$$\bar{r}^m - \bar{r}_0^m = \alpha t \text{ --------------------- (1.1)}$$

where $\bar{r}$ is the average grain size after time t and $\bar{r}_0$ is the average initial grain size and α follows equation 1.2.

$$\alpha = \alpha_0 \exp\left(-\frac{Q}{kT}\right) \text{---------------- (1.2)}$$

and m is normally expected to be 2 but is found be somewhat higher.

For thin films if the as-deposited grain structure has equiaxed structure smaller than the film thickness then it evolves by normal grain growth. This leads to a monomodal grain structure. However, the grain growth slows down and stops as the grain size approaches the film thickness [bec49, Pal47]. This stagnation is associated with formation of thermal grooves which adds a thermal drag slowing and eventually stopping grain growth [Mul87].

Sometimes secondary grain growth takes place which leads to a bimodal size distribution [Wie03]. This happens when the driving force for grain growth acts selectively. The main reason for such selectivity is anisotropy of surface energy, interface energy and/or strain energy. Presence of precipitates can also lead to abnormal grain growth in films [Doh87].

1.2.2 Grain growth in presence of moving heat zone

Simulations with grain boundary mobility varying in space and time have been found to lead to unusual microstructures [Hol98, Hol91]. From such simulations, a scanning gaussian heat profile leads to normal grain growth locally but very little grain growth in any other region and as the heat front is scanned the grain boundary is pushed in the direction if scanning, leading to large grains. If the scanning rate is sufficiently low, the grain boundary can be pushed ahead of the heat front leading the very large grains/ near single-crystal structures [Hau01].

The scanned laser annealing of patterned Al and Cu films is known to lead to three regimes

a) Agglomeration
b) Bamboo grain structure
c) Polygranular structure

depending on the power of the laser and the scanning velocity [Hau99, Hau00].

For both Cu and Al films, at higher powers agglomerated structures are formed. At lower powers bamboo structure is formed at lower scanning rates while polycrystalline structures were formed at higher scanning rates as shown in Fig 1-1, 1-2.

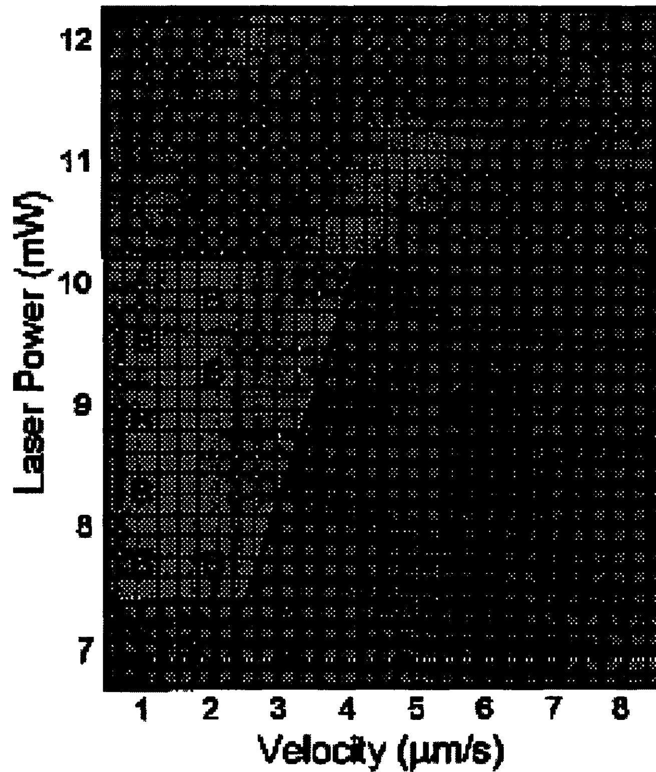

Fig1-1 Microstructural map of the microstructure regimes defined by laser power and scan velocity for Al. The final microstructure are agglomerated(X), bamboo (B), and polygranular (P). [Hau99]

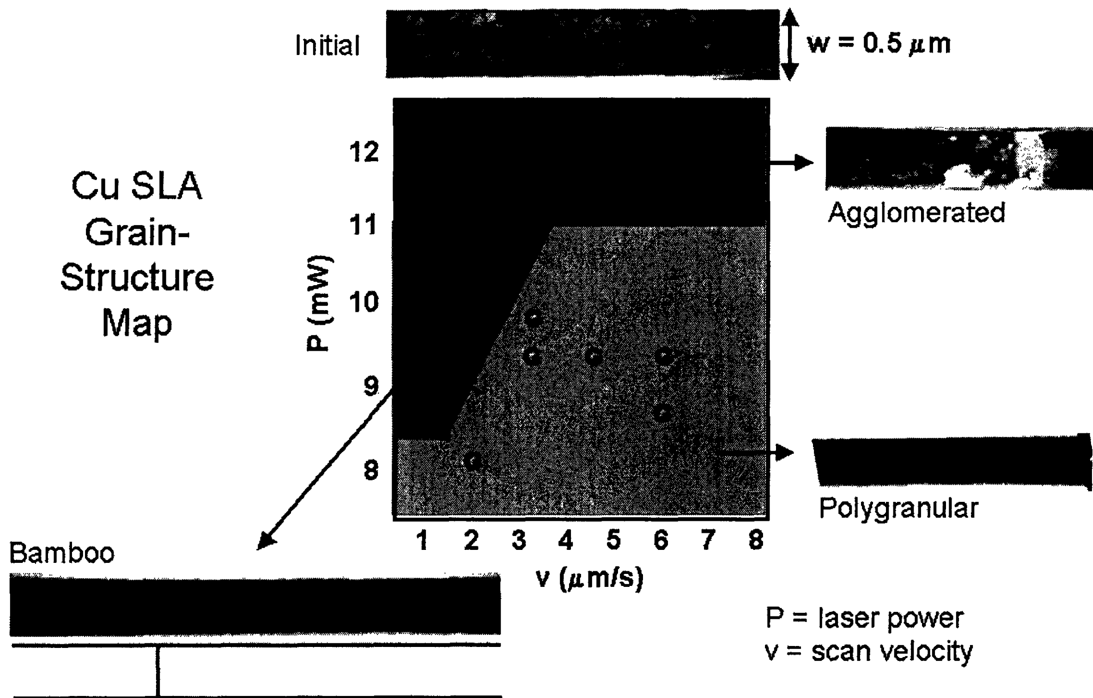

Fig1-2 Microstructural map of the microstructure regimes defined by laser power and scan velocity for Cu. The final microstructure are agglomerated(X), bamboo (B), and polygranular (P) [Hau00].

The average grain length formed by scanned laser annealing is also known to increase with increasing power and decreasing scan rates as shown in Fig 1-3, 1-4 [Hau99, Hau00].

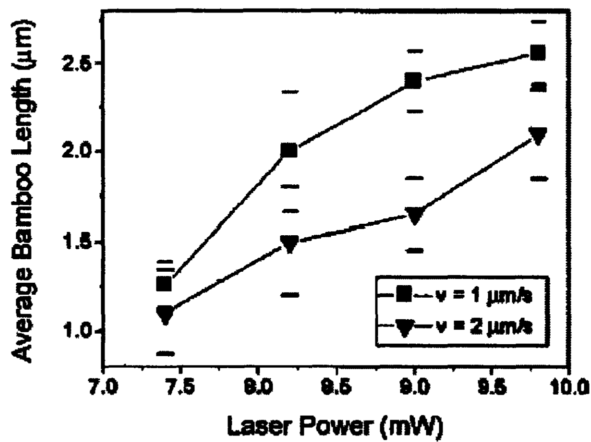

Fig1-3 Plot of dependence of the average bamboo grain length as a function of laser power and scan rate for fully bamboo structures in Al [Hau99].

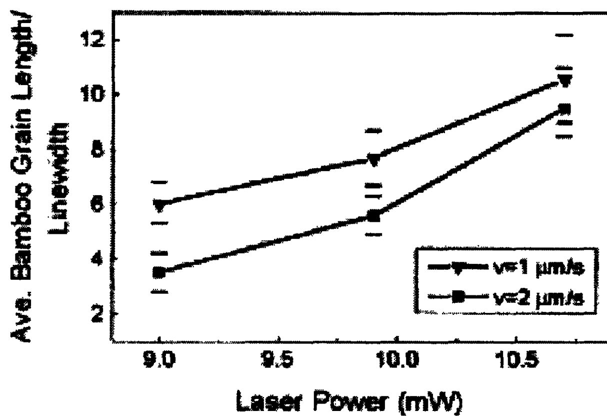

Fig1-4 Plot of dependence of the average bamboo grain length as a function of laser power and scan rate for fully bamboo structures in Cu [Hau00].

This dependence of final microstructure on power and scanning velocity has also been observed in simulation of scanned laser annealing (Fig 1-5) [Hau01].

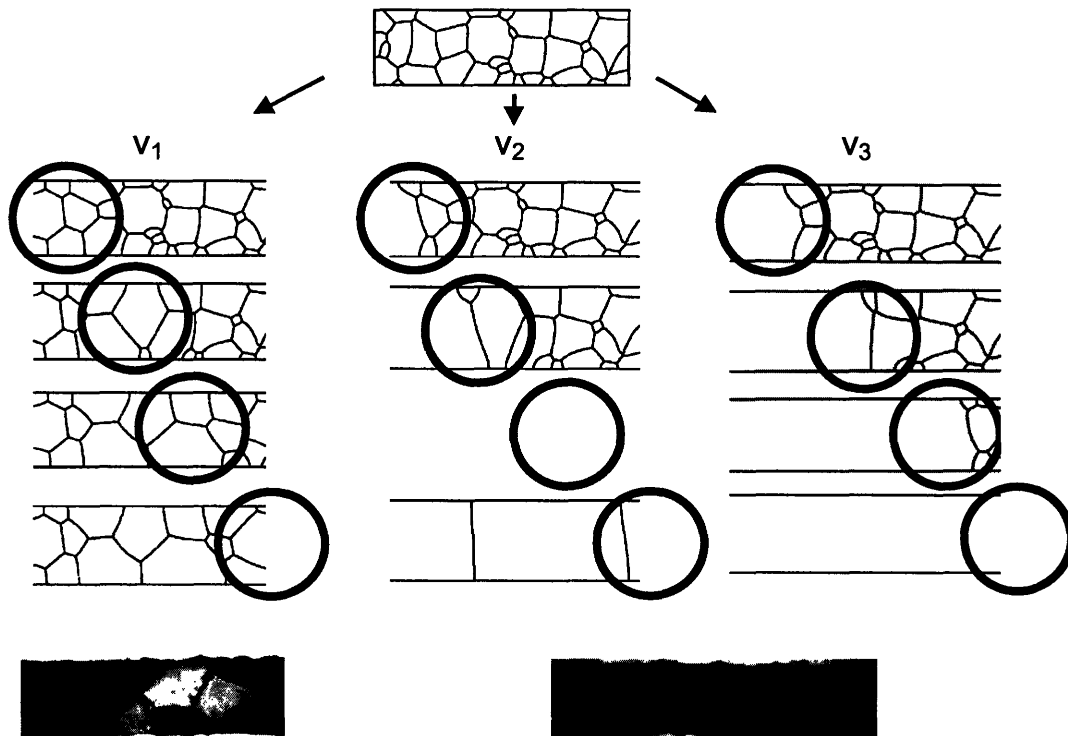

Fig 1-5 Various microstructure regimes depending on scanning velocity (Simulations) [Hau01]

Through simulation of grain growth induced by scanned laser annealing, it is known that thermal gradient along the scanning direction is an important parameter that influences the final structure. Steep thermal gradient lead to longer average bamboo grain lengths in patterned lines [Hau01] (Fig 1-6).

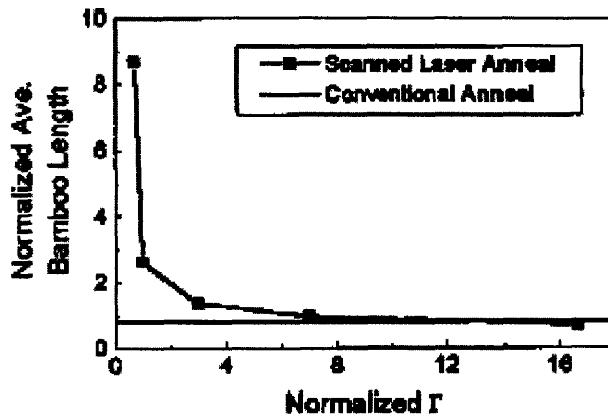

Fig1-6 Grain growth simulation showing that a steeper thermal gradient, or a smaller Γ, leads to longer bamboo grain lengths. Γ is defined such that the thermal profile along the scanning direction(x axis) fits the equation $T = T_0 + (T_{max} - T_0)\exp\left(\frac{-(x-x_0)}{\Gamma}\right)$ [Hau01]

Three key variables that influence the microstructure evolution by scanned laser annealing are:

1) Power
2) Scanning velocity
3) Thermal gradient

1.3 Motivation for the present work

Thin metallic films are used for many applications including semiconductor industry metallization, and MEMS. The grain size and texture can significantly affect the performance. As explained earlier, the grain size and texture can be influenced both by pre-deposition condition and the post-deposition processing.

AS the microelectronics industry has moved into Cu as the conductor material, there has been a lot of thrust in research into microstructure control in Cu thin films. The grain size influences the resistivity of conductor because of grain boundary scattering [May]. As the line width reduces below 100nm, the grain boundary scattering is primarily responsible for the resistivity increases in the conductor [Sti02]. The surface scattering is important too, but not dominant as shown in Fig 1-7. This resistivity increase is a major concern since it leads to RC losses beyond those projected [ITR04]. It is very difficult to get grains to grow in these very narrow lines, because of the impurities from electrodeposition, but more fundamentally, because bamboo grain sizes by conventional annealing are limited by the minimum dimension.

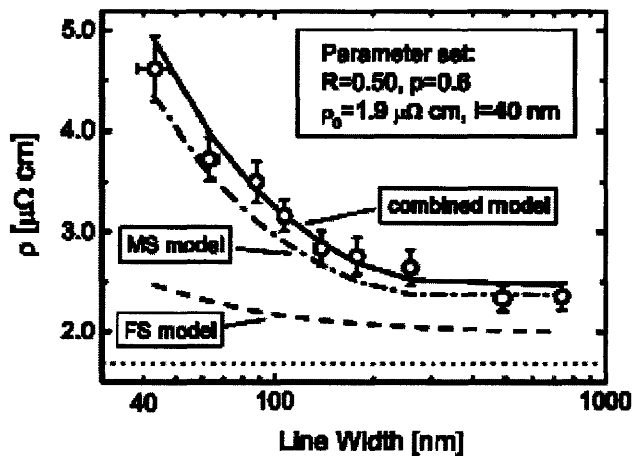

Fig 1-7 Resistivity increase as the line width decrease (FS model accounts for the surface scattering as size goes down, and MS model accounts for the grain boundary scattering) [Ste02]

Large grained structures would have low grain boundary scattering and are thus ideal candidates for conductors. Final grain sizes produced by conventional anneals depend on the line dimensions. Therefore, in any experimental study which tries to explain the increase in resistivity as the line width shrink, it is very difficult to isolate the effect of grain boundary scattering from surface scattering due to reduced dimensions. Scanned laser annealing could be a very effective tool to produce grain of different sizes for the

same line dimensions and thus structures could be made to quantify the effect of grain boundary scattering.

In Al based interconnects the electromigration mechanism is well known. The grain boundary acts a high diffusion paths for atoms and therefore there is a very strong dependence of the reliability on the microstructure of the interconnect. Bamboo lines with grain boundaries perpendicular to the line are known to have lifetimes orders of magnitude more than the interconnects with polycrystalline structures.

As Industry has moved to Cu-based interconnects, new mechanisms have been identified to be the responsible for elecromigration. The interfacial diffusion between the conductor and the surrounding barrier layer provide the high diffusivity path. The barrier-Cu interface also acts as sites for easy stress-induced voiding and consequent void growth by electromigration. Since interfacial electromigration is the dominant mechanism, the crystallographic orientation of the grains could influence the reliability.

Scanned laser annealing could be used to develop test structures with extremely large grains such that the vias contacted single grains. This could be used to study the crystallographic dependence of the rate of interfacial electromigration and voiding at Cu-barrier interfaces. Such study could be used to decide the processing methods and to make structure-sensitive reliability projections for interconnects.

For making extremely large grained structures the role of thermal gradient in scanned laser annealing should to be further studied and a scheme to alter the thermal profile should be implemented. Several methods could be used to alter the thermal profile. An active cooling of substrate could alter the thermal gradient significantly. Change in kind of substrate such that the effective thermal conductivity and specific heat is changed, can also alter the thermal profile. The latter scheme is implemented in the present work. Two sample, one with Cu film over Si substarte with a silicon oxide layer and the other with Cu film over Si substrate over just the native oxide, were compared.

Chapter 2

Experiments

2.1 Laser Set-up

A schematic of the laser set-up is shown in Fig 2-1. A diode pumped and frequency doubled ND: YLF laser (Spectra Physics 7960-L4-E / 7965-L4) which emits light at green wavelength (523nm) was used. The beam was then collimated using collimating lenses and the reflected by dichroic mirror. Dichroic mirror reflect only the green wavelength which allows the illumination of the sample by white light for viewing in situ by a camera system. Beam was focused at normal incidence onto the sample by focusing objective lenses. The diode pump power, the mode of operation (continuous wave or pulsed) and pulsing frequency (in pulsed mode) could be controlled by the Model 7310 remote control. A variable neutral density neutral density filter was added in the beam path to gain better control of the beam power.

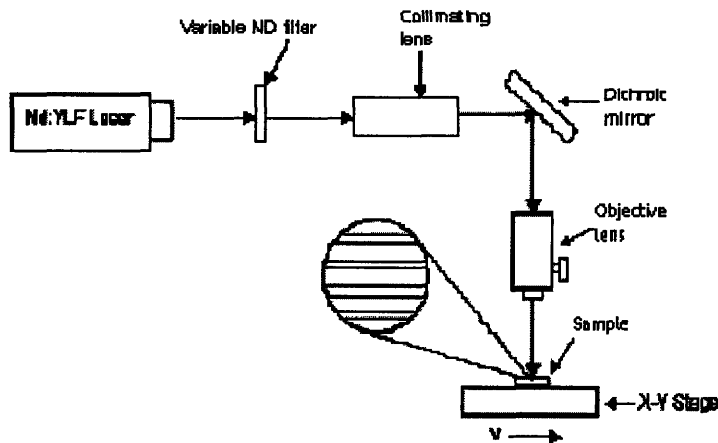

Fig 2-1 Schematic diagram of scanned Laser annealing set-up[Hau01(modified)]

The sample was attached to an x-y stage which c be moved at velocities slower than 1μm/sec. The motion is controlled by Newport K82 actuators that were programmed by the motion control module (PCM-400).

2.2 Samples

Fig 2.2 (a),(b) shows a schematic diagram of the samples used. There were two kind of samples used for the experiments.

a) Cu(3000A)/Ta(200A) films on 150mm-diameter and 650μm thick (100) Si wafers.
b) Cu(3000A)/Ta(200A) films on 150mm-diameter and 650μm thick (100) Si wafers coated with 1.5μm-thick silicon dioxide deposited using PECVD.

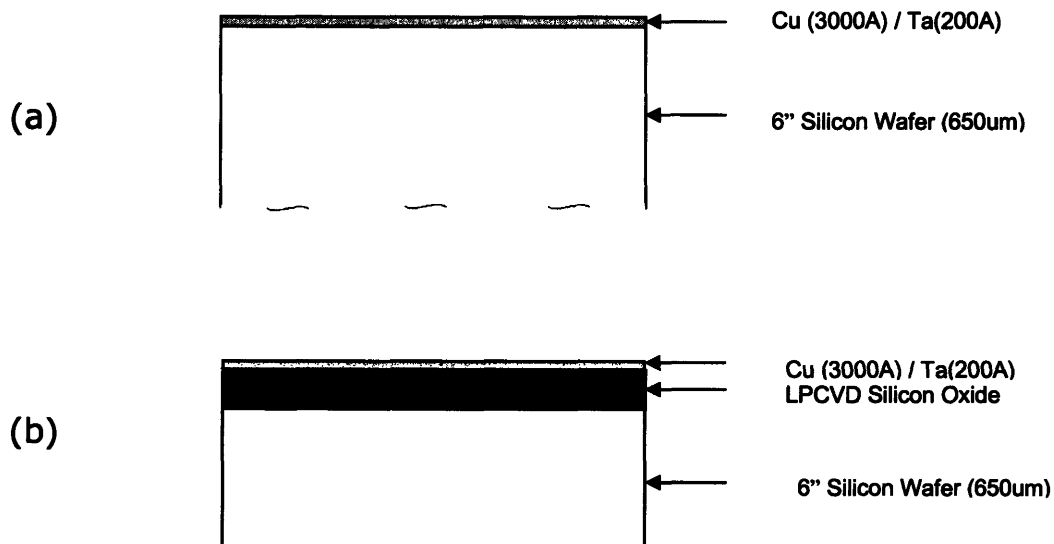

Fig 2-2 (a) Sample without the oxide layer **(b)** Sample with the oxide layer

Cu thin film was deposited on both kinds of substrates. A barrier layer to prevent copper diffusion into silicon dioxide or silicon was deposited before Cu. Tantalum was chosen as a diffusion barrier and an adhesion promotion layer for copper metallization. The metals were deposited using physical vapor deposition (PVD) in an e-beam evaporative deposition system. Ta was deposited first, followed by Cu without breaking vacuum. The chamber base pressure was around 2E-6 torr for the deposition.

2.3 Laser Scanning and Analysis

The samples were scanned at three different velocities 1μm/sec, 5μm/sec and 60μm/sec and over a range of powers. The range of power was experimentally determined so that all the regimes of laser processing of Cu film were present and it was implemented by adjusting the variable neutral density filter.

In each scan, the velocity was constant and power was decreased in steps at uniform intervals. Several places in the scan were deliberately marked by the laser and these marks were later used during analysis to easily determine power at any location. Pulsed mode at pulsing frequency of 7 KHz was used for the scans. A few scans were done at different pulsing frequencies. These scans were done for a good comparison to determine the effect of thermal gradient on microstructure evolution by scanned laser annealing. It will be described in more detail in the chapter on thermal modeling.

All the studies on the effect of Laser processing on these samples were done using Scanning Electron Microscope (Phillips XL30) and Focused Ion beam Microscopy (FEI dual beam FIB).

Focused ion beam microscopy can create good contrast between grains of different orientation because of channeling effects of Ions. Another advantage of FIB microscopy is that there is no sample preparation involved and therefore it was chosen as a tool to study the microstructure before and after laser processing. Typical ion-beam current used

for microscopy was 30pA. At this current, a good contrast was obtained and milling due to the ion beam was minimal. CDME detector was used to get a better contrast in the images.

Chapter 3

Thermal Modeling

3.1 Introduction

ADINA 8.0, a finite element modeling tool, was used to do the thermal modeling of the laser scanning process. Fig 3-1 is a captured screenshot from ADINA showing the geometry used. A simple analysis for a single pulse was performed. Only a small area of the substrate, a cylinder 30 μm in radius and 50 μm in height was used to simplify the analysis and this geometry also represents the worst scenario for cooling. The boundary condition on all the surfaces was fixed at zero flux. The thin adhesion layer was also removed so that the structure could be meshed more effectively. The adhesion layer has a high thermal conductivity and a small thickness and is therefore unlikely to affect the results significantly. ADINA does not accept analytical forms for the flux loading profile, therefore the Gaussian beam profile was approximated by a polygon with calculated values of gaussian profile.

	Density(Kg/m3)	Conductivity(W/mK)	Specific heat(J/KgK)	Reflectivity(% at 523 nm)
Cu	8960	400	385	70
Si	2330	150	840	NA
SiO_2	2300	1.1	722	NA

Table 3-1 Material properties used in FEM analysis.

The general equation for conduction of heat in a solid without heat sources or sink is

$$\frac{\partial T}{\partial t} = \frac{k}{\rho C_p} \nabla^2 T \quad \text{----------------------} \ (3.1)$$

where T is the temperature, t is the time, k is the thermal conductivity, ρ is the mass density, and C_p is the specific heat. This equation (3.1) is used by the FEM solver and the material properties used is shown tabulated in Table3-1.

Heat flux can be applied as a boundary condition in the equation. For the present analysis, the flux was applied on the Cu surface. A transient Thermal Analysis was performed. Reflectivity was taken into account by calculating the effective power by equation 3.2.

$$Effective_power = P(1 - R) \quad \text{------------} \ (3.2)$$

P is the power of the laser beam and R is the reflectivity.

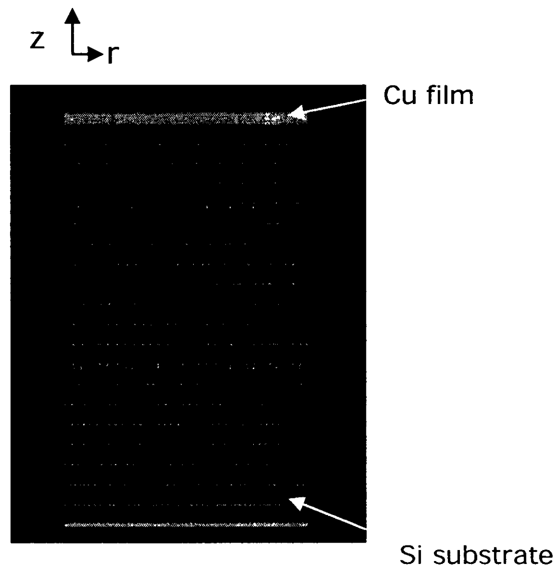

Fig 3-1 Geometry for FEM analysis: Cylinder 30μm radius 50 μm height
Axis symmetric element with z axis as the axis of rotation
(Zero flux boundary conditions on all walls were assumed, to simulate worst-case conditions for cooling.)

Axis symmetric elements about the z-axis were used for meshing.

3.2 Results

The cooling curves for a single-pulse analysis for the samples with no oxide and the samples with oxide layers are shown in fig 3-2(a), (b). These cooling curves are for a point near the surface of Cu film and at the center of the beam.

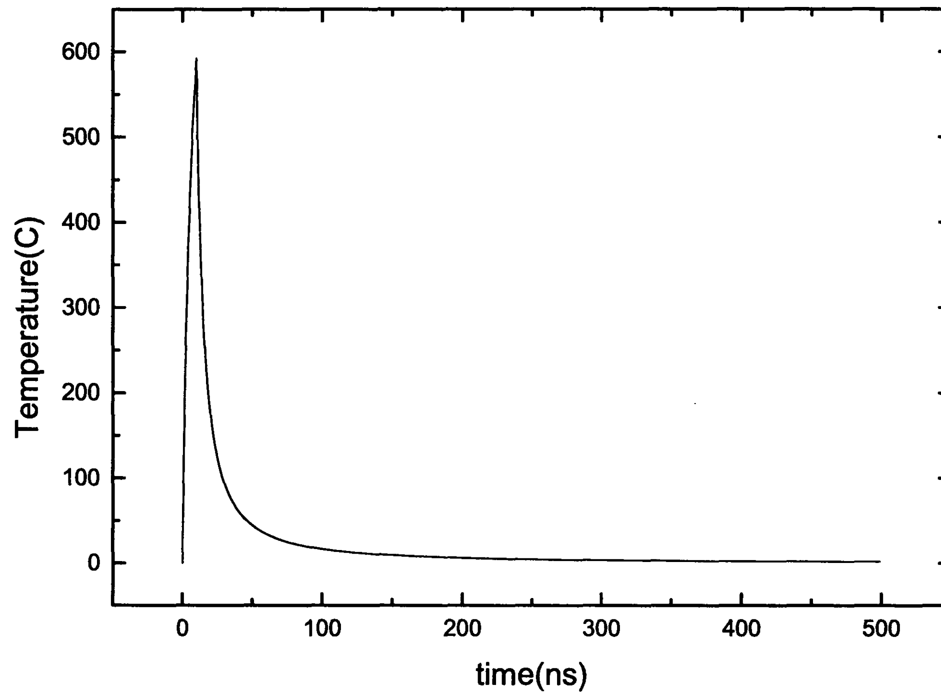

Fig 3-2(a) Cooling curve at the center of the beam for sample with no oxide layer T vs. time

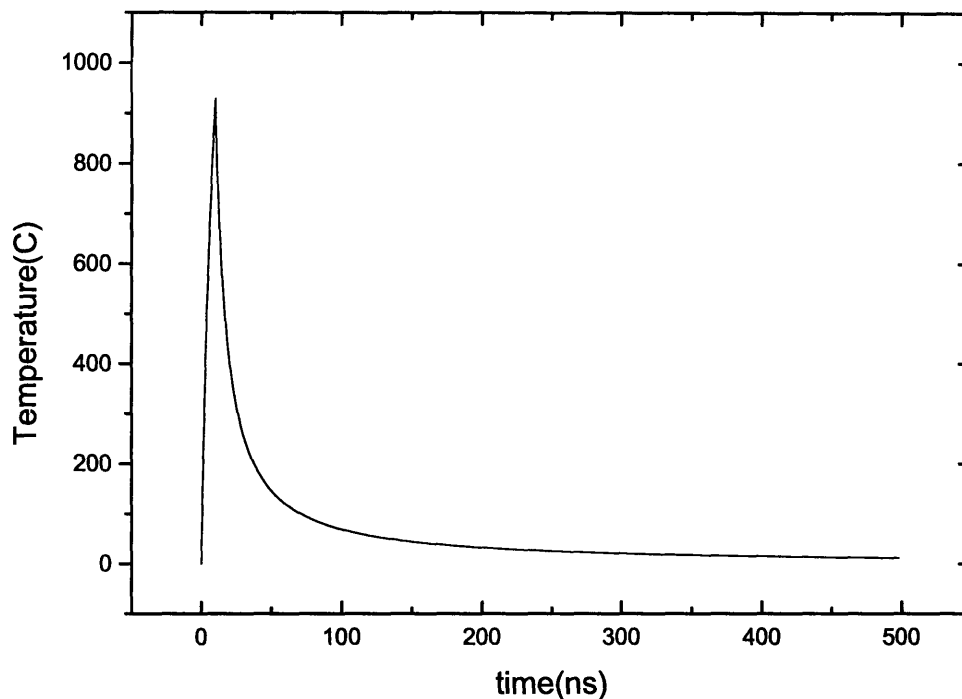

Fig 3-2(b) Cooling curve at the center of the beam for sample with an oxide layer T vs. time

The cooling times determined from this analysis are of the order of nano-seconds while the separation between the pulses is of the order of milliseconds. Therefore pulses are independent of each other. A single pulse analysis can give the temperature-time diagram that a point goes through and the same condition is repeated over pulses.

For the same power pulse, the peak temperature for a sample with an oxide layer is higher than the peak temperature for a sample without an oxide. The oxide layer has a low thermal conductivity and a high specific heat and therefore the heat is localized in the Cu film, so that it is intuitively correct that it goes to higher temperatures.

The cooling times associated with a sample with an oxide layer were found to be longer than a sample without oxide layer. This can be understood by the same reasoning that the

low conductivity and high specific heat oxide layer prevents leakage of heat from the Cu film, which could otherwise be lost into the substrate quickly.

3.3 Equivalent conditions to study the effect of thermal gradient on grain growth

There is a temperature-time disparity in the cooling of the two samples as discussed in section 3.2. Therefore to create equivalent conditions for the two samples, the power was scaled down for the oxide sample to get the same peak temperature. The cooling times associated with the two samples were still different and in order to create an equivalent condition for studying the effect of the thermal gradient, the pulsing frequency was reduced in the case of the sample with an oxide layer.

For equivalent points:

(a) the power for the sample with an oxide was scaled down to get same maximum temperature, and

(b) the pulsing frequency of the laser in the case of the sample with an oxide layer was scaled down to compensate for longer cooling times.

3.3(a) Scaling of Power

A number of simulations were run with different powers for the sample with an oxide layer and the maximum temperatures attained were found to be proportional to the power. This result is expected because the heat is highly localized in the Cu thin film. The scaling to obtain the same maximum temperature for the samples without an oxide layer requires a simple proportional scaling of input power. The cooling curve of the sample with an oxide layer after the scaling is shown in fig 3-3.

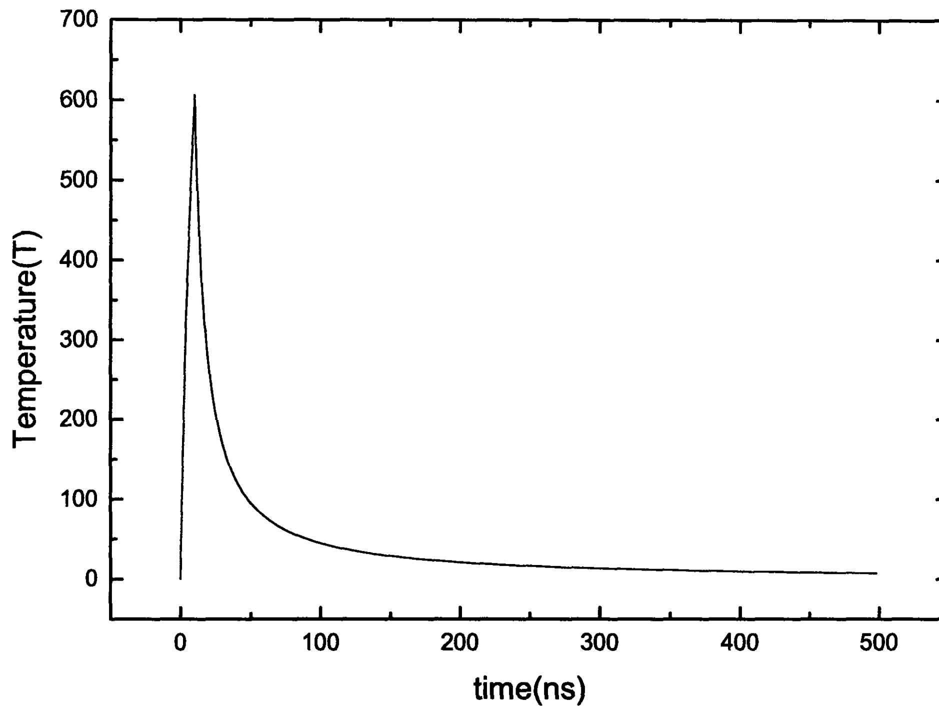

Fig 3-3 Cooling curves after adjusting powers (Power in sample with oxide scaled down): T vs. time.

3.3(b) Scaling of Pulsing frequency

3.3(b).1. Introduction

A comparison of cooling curves for the sample with an oxide layer after scaling of power, and the sample without the oxide layer was done (fig 3-5). The maximum temperature attained in both cases is same, but the cooling time in the sample with an oxide layer is longer. This made any comparison between the two samples incorrect. For a good comparison between the two samples the "thermal dose" should be made equal.

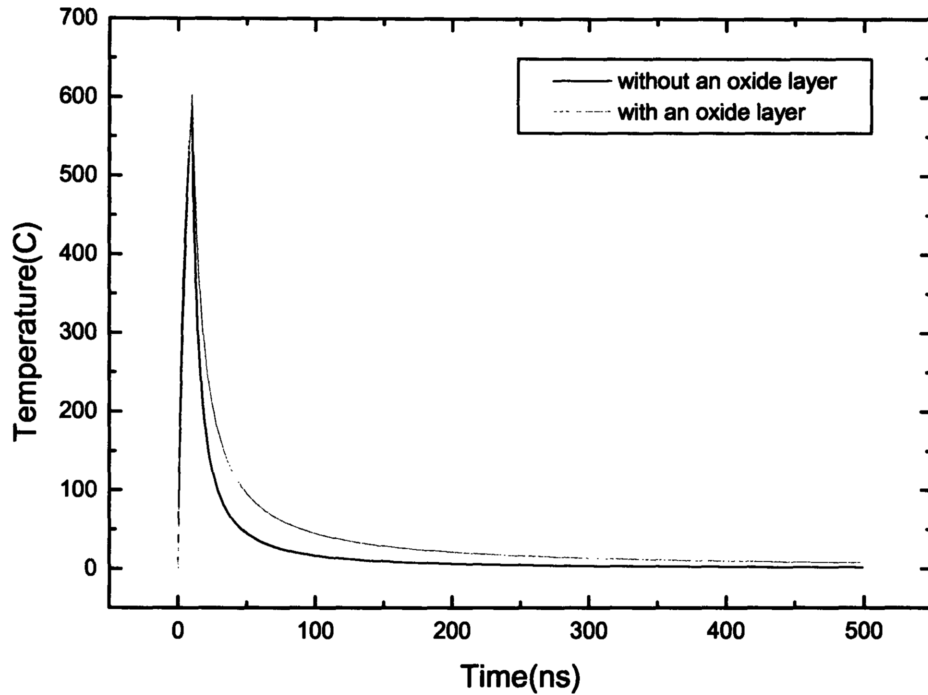

Fig 3-4 Comparison of the cooling curves after scaling of powers.

3.3(b).2. MATLAB Simulations for Grain Growth and Thermal Dose

A simple equation that can estimate the grain growth while accounting for the temperature dependence of grain boundary mobility is

$$\frac{dA}{dt} \propto D_{gg} e^{\left(-\frac{E_{gg}}{kT}\right)}$$. ------- (3.3) [Tho90]

From the cooling curve, the temperature-time data was extracted and a numerical integration was run in MATLAB to estimate the grain growth by equation (3.2)

$$\Delta A \propto \int D_{gg} e^{\left(-\frac{E_{gg}}{kT}\right)} dt \qquad \text{-------- (3.3)}$$

The "thermal dose" for comparison of grain growth between the two samples was considered proportional to the grain growth estimated using equations (3.2) and (3.3) as formulated in equation 3.4.

$$TD = \Delta A \times \left(\frac{S}{V}\right) \times \nu \qquad \text{-------- (3.4)}$$

Where S is the spot size and V is the scanning velocity, and ν is the pulsing frequency. $\left(\frac{S}{V}\right)$ is the dwell time of the beam at a spot, and $\left(\frac{S}{V}\right) \times \nu$ is the number of pulses that hit a spot.

The pulsing frequency in the sample with no oxide was scaled according to following equation to make the thermal doses equal.

$$\frac{\nu_{ox}}{\nu_{noox}} = \frac{TD_{ox}}{TD_{noox}} \qquad \text{------- (3.5)}$$

Where ν_{ox} and ν_{noox} denote the pulsing frequencies for a sample with an oxide layer and a sample without an oxide layer respectively and TD_{ox} and TD_{noox} are the thermal doses for the two samples.

The temperature gradient is higher for the sample without an oxide layer. Without the oxide layer the heat can leak into the substrate more effectively and therefore the temperature dies down quickly, not giving enough time for heat to spread in the scanning direction leading to lower transverse thermal gradients in that direction as illustrated in Fig 3-5.

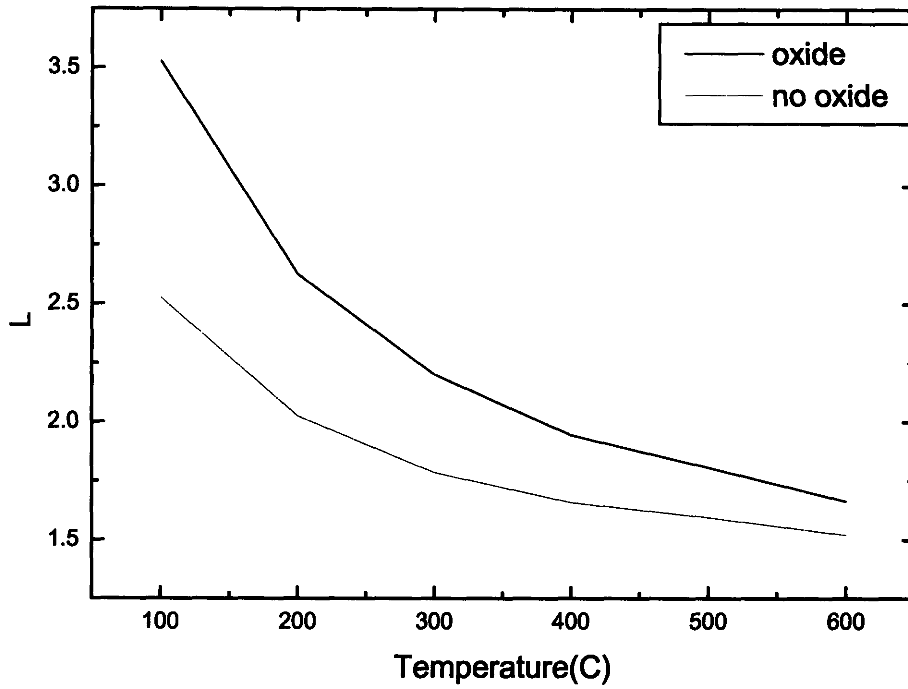

Fig 3-5 Thermal gradients in the scanning direction, L is defined such that the thermal profile along the scanning direction(x axis) fits the equation

$$T = T_0 + (T_{max} - T_0)\exp\left(\frac{-(x - x_0)}{L}\right)$$

Chapter 4

Results and Discussion

4.1. Regimes

At all scan velocities and in both sample types, three regimes were identified

1) Ablation
2) Agglomeration
3) Grain Growth

The powers at which these regimes occurred varied with scanning velocity and the type of sample. The powers at which these regimes occur for different velocity for the sample without oxide layer is plotted on fig 4-1(a) and the sample with the oxide layer is plotted on fig 4-1(b).

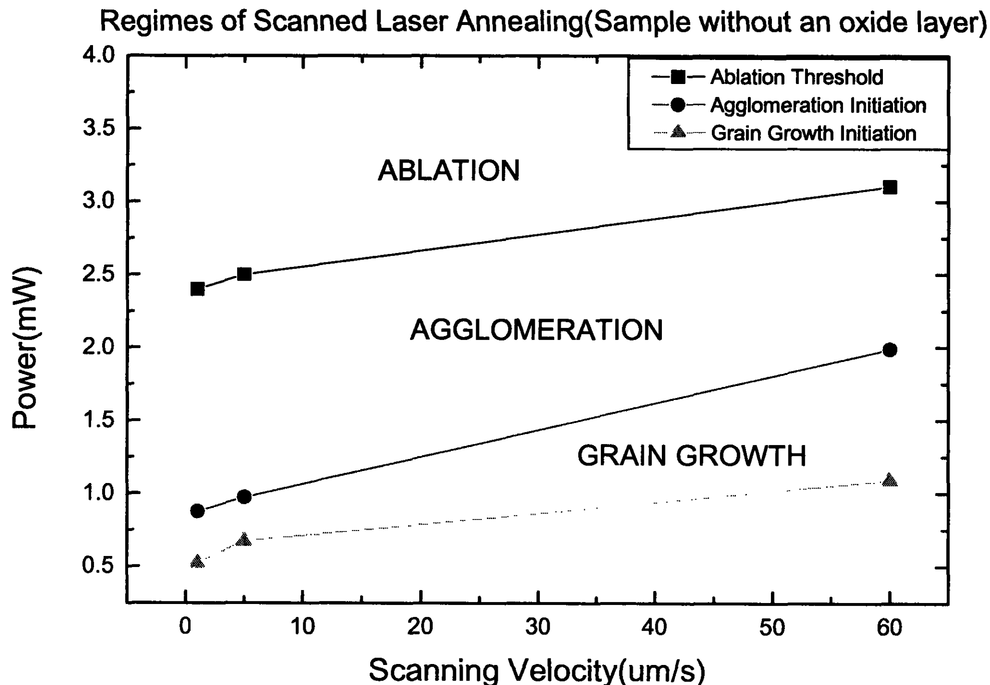

Fig 4-1(a) Regimes of Scanned laser annealing for sample without any oxide layer.

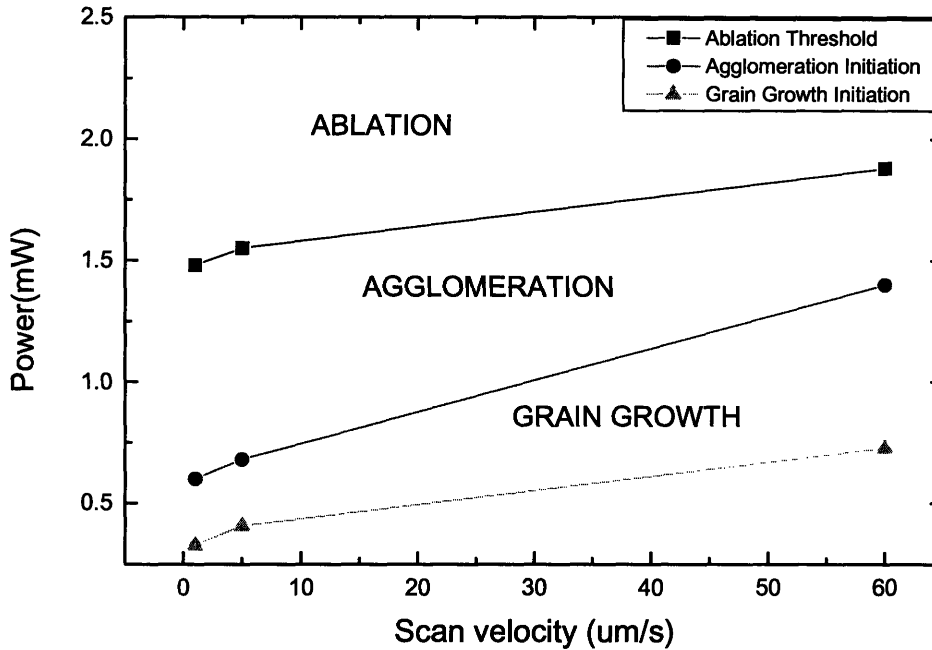

Fig 4-1(b) Regimes of Scanned laser annealing for sample with oxide layer.

Each regime will be discussed in the later sections. On the whole, the powers at which these regimes occur seem to shift towards lower power for the sample with oxide layer. This is expected because of the poor cooling and hence higher maximum temperatures attained in sample with an oxide layer as discussed in Chapter 3. The shifts and checking its consistency with the thermal model will be delved upon in the sections that follow

4.2 Ablation

The powers at which ablation was observed is shown in fig 4-1 (a), (b). This regime was observed at high powers in all the scans. Some images of ablation are shown in fig 4-2. The threshold for ablation showed a weak dependence on velocity and it was found to

increase as the velocity increased. The thresholds for ablations at all velocities shifted towards lower power in the sample with an oxide layer.

The maximum temperature for the threshold powers was extracted from the thermal modeling. For each velocity, the maximum temperatures reached at threshold powers was very comparable for the sample with oxide and sample without oxide as shown in table 4-1. This validates the thermal modeling.

Velocity	$R = T_{ox}/T_{noox}$
1um/s	1.081
5um/s	1.075
60um/s	1.1

Table 4-1 Ratio of maximum temperature attained at the ablation threshold for the sample with oxide layer and the sample with no oxide layer at different velocities.

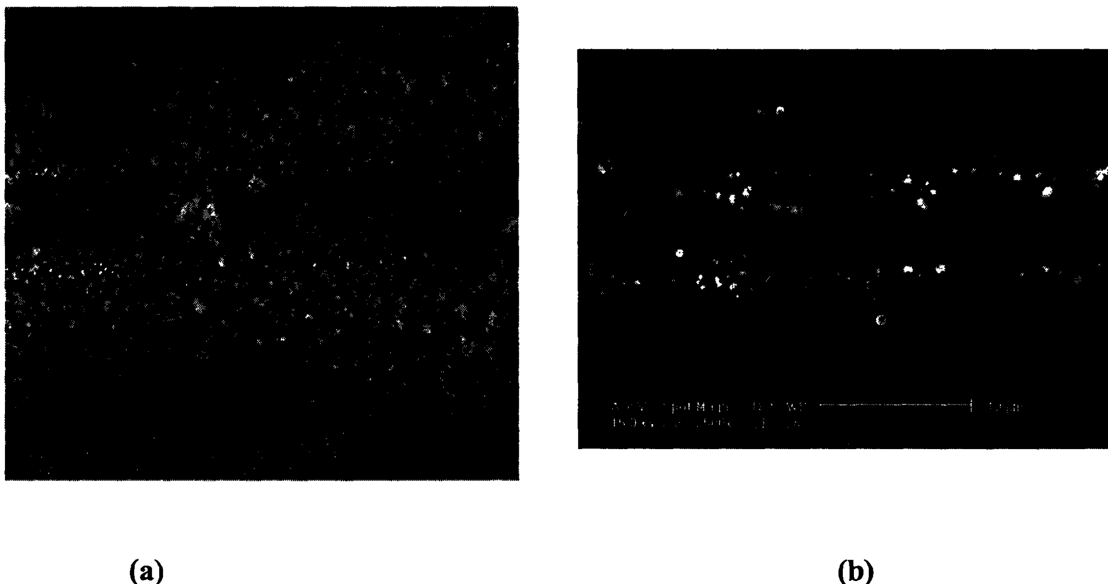

(a) **(b)**

Fig 4-2 Images of ablated region (a) at P = 1.9W, v = 1 μm/s, sample with an oxide layer (b) at P = 2.8 W, v = 1 μm/s, sample without an oxide layer.

4.3 Agglomeration

At powers below the ablation threshold, a regime was observed where agglomerated structures are formed as shown in fig 4-1(a), (b). The powers at which these agglomerated structures were observed shifted towards higher power as the velocity increased. For all the velocities the regime shifted towards lower power for the sample with an oxide layer.

These agglomerated structures were quasi-periodic. The period of these structures was found to decrease as the power was increased and as the velocity was decreased. A graph of how the structures looked as the power was changed and over different velocities is shown in figure 4-3(a), (b).

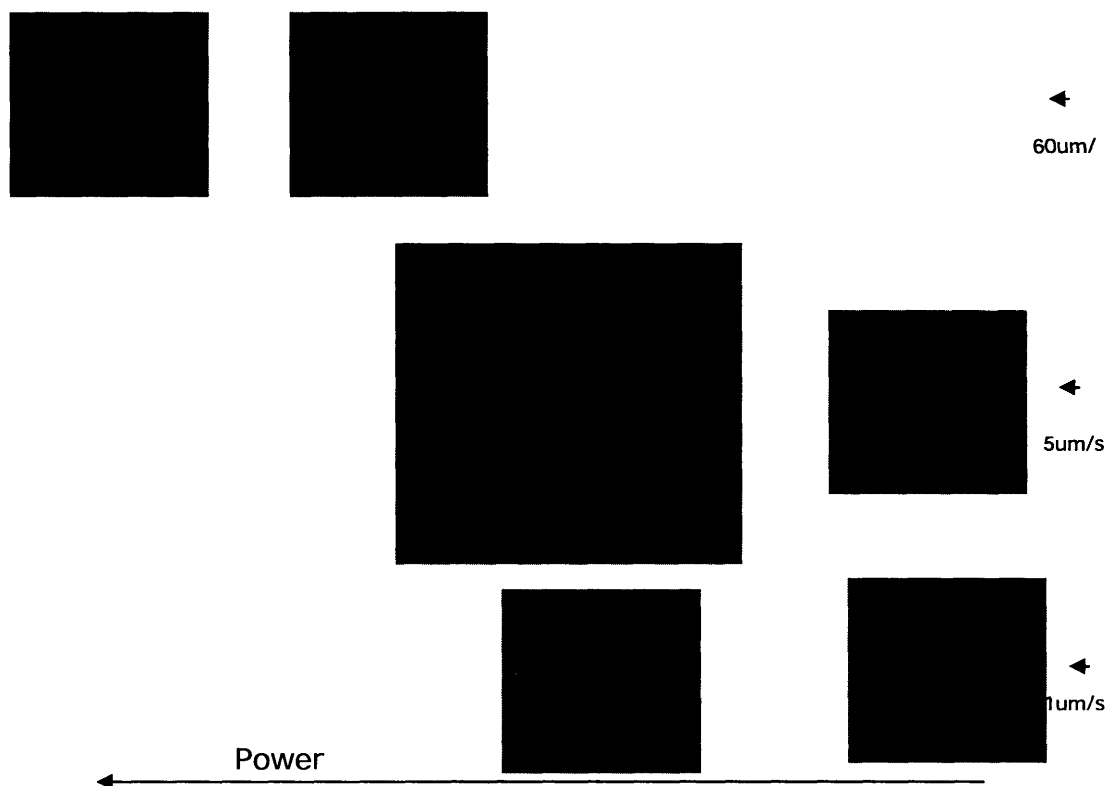

Fig 4-3(a) Agglomerated structures over different power and velocities for the sample .without an oxide layer.

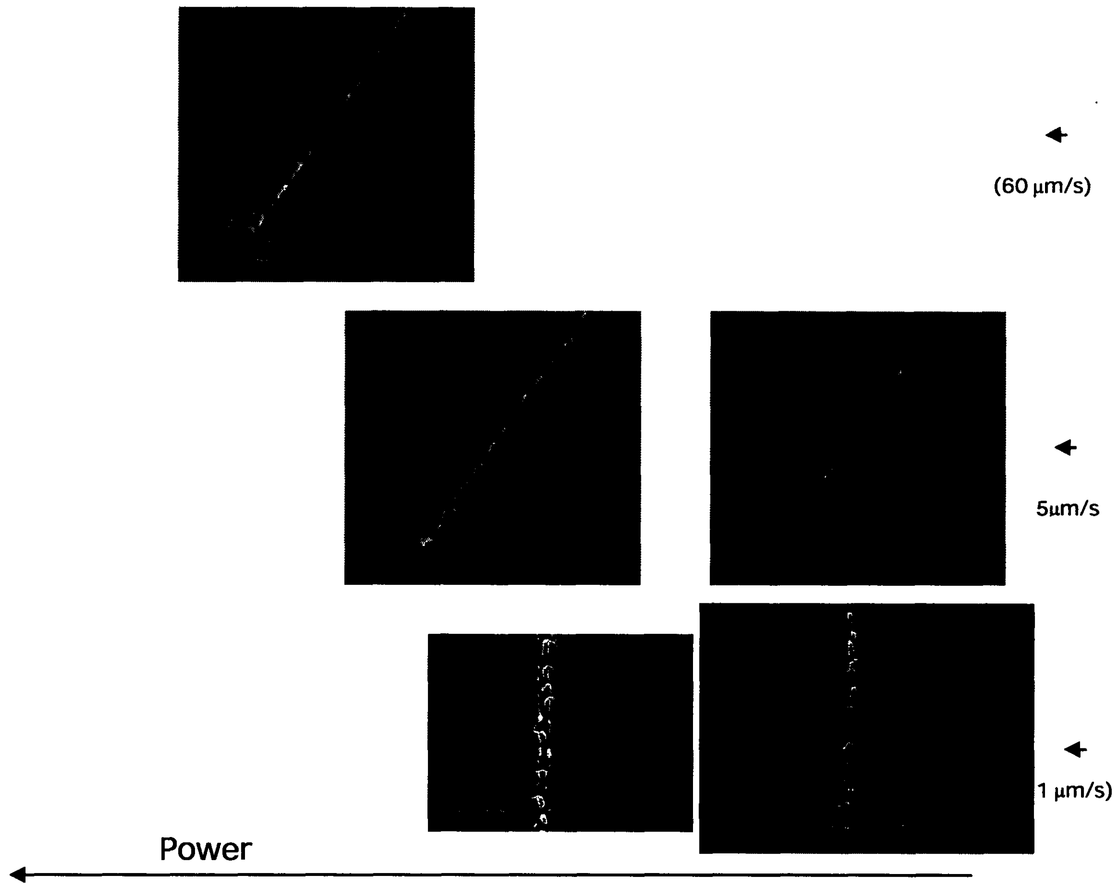

Fig 4-3(b) Agglomerated structures over different power and velocities for the sample with an oxide layer.

4.4 Grain Growth

4.4.1 Effect of Power and scanning velocity

At powers lower than those at which agglomeration occurs there was a regime in which grain growth was observed as shown in fig 4-1(a), (b). The range of powers at which grain growth was observed shifted towards higher power as the velocity increased. A graph of how the structures looked as the power was changed and over different velocities is shown in figure 4-4(a), (b).

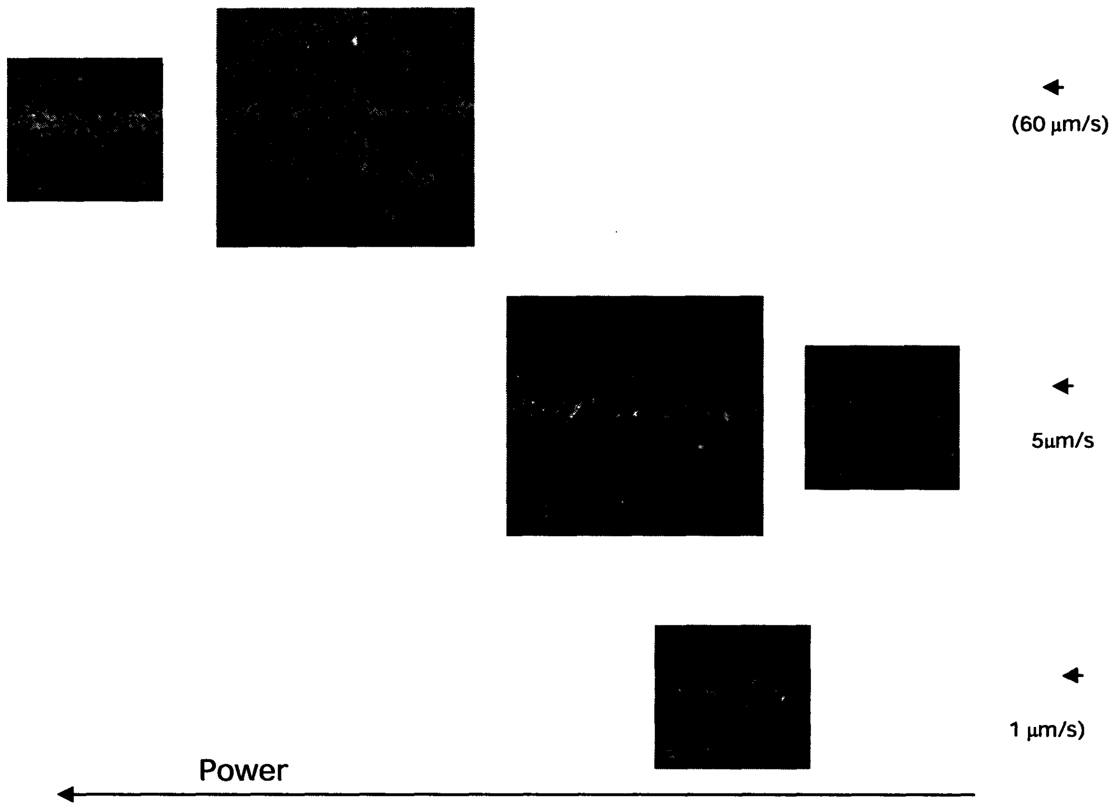

Fig 4-4(a) Grain growth over different power and velocities for the sample without an oxide layer.

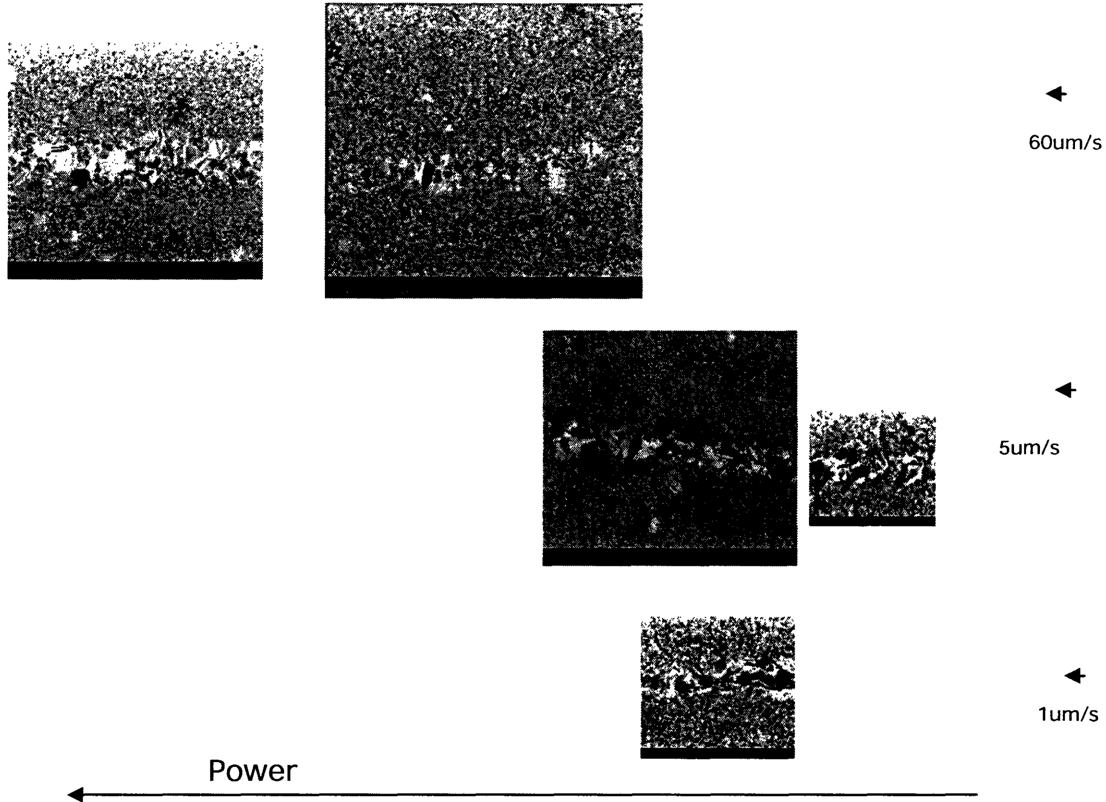

Fig 4-4(b) Grain Growth over different power and velocities for the sample with an oxide layer.

The regime was also observed to shift towards lower powers in the sample with an oxide layer. For both the samples, the average grain size was found to increase with decreasing scanning velocity and increasing power. This is expected because increasing power increases the temperature and hence the mobility of the grain boundary and thus leads to more grain growth, while decreasing the velocity leads to more time at the temperature and hence more grain growth.

4.4.2 Effect of the thermal gradient on the Grain growth

As described earlier in chapter 3 on thermal modeling, the thermal gradient is expected to be more in the sample without an oxide layer compared to the sample with an oxide layer. This is expected to influence the grain growth during scanned laser annealing of these samples. However, a good comparison between the two samples could only be done after scaling of power and pulses to account for the higher temperatures and cooling time in the sample with an oxide layer. The scaling scheme has been described in detail in the chapter on thermal modeling (chapter 3).

Three samples were compared at three conditions:

1) v = 1 μm/s, P= 0.65W, for sample without an oxide layer (Fig 4-5)

2) v = 5 μm/s, P= 0.65W for sample without an oxide layer (Fig 4-6)

3) v = 60 μm/s, P = 0.86 W for sample without am oxide layer (Fig 4-7)

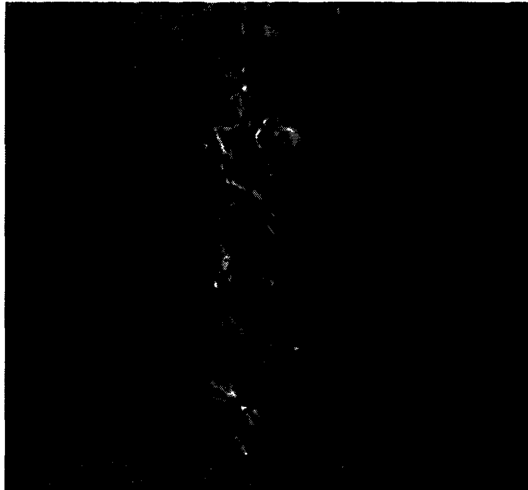

Sample with an oxide layer

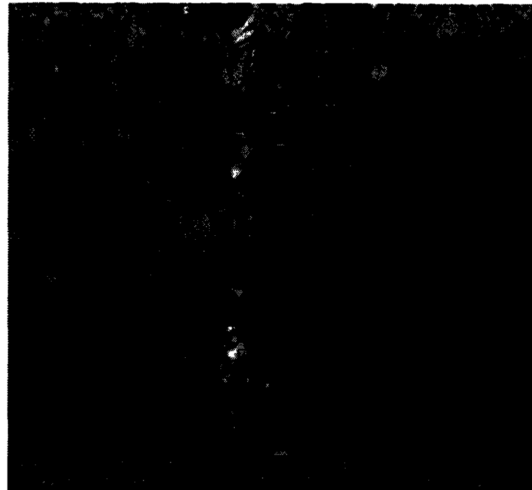

Sample without an oxide layer

(a) Low magnification image 10KX

Sample with an oxide layer

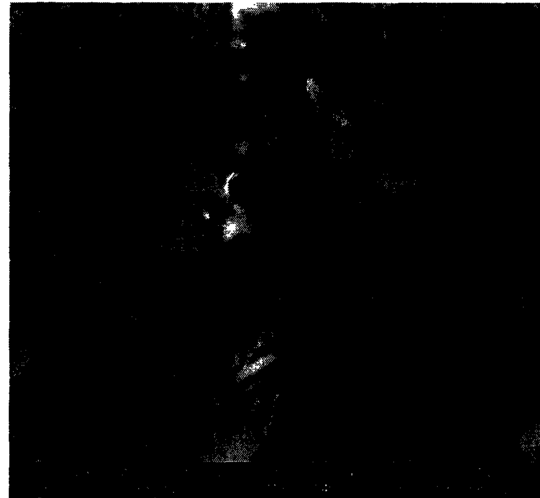

Sample without an oxide layer

(b) High Magnification image 20KX

Fig 4-5 (a) and (b) Comparison between grain growths at equivalent points in the two samples for scanning velocity of 1 μm/s.

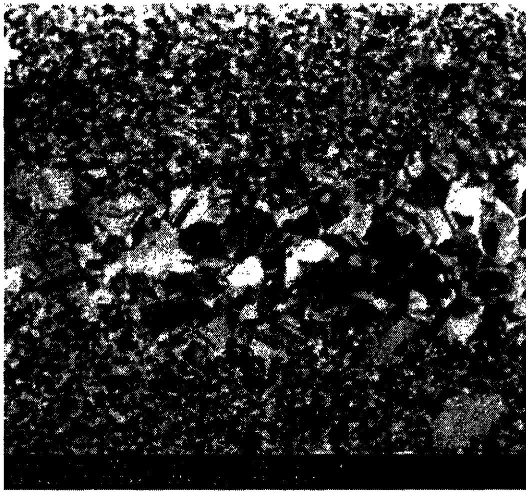

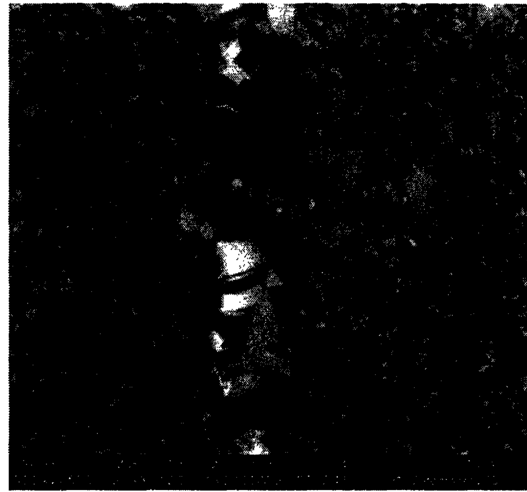

Sample with an oxide layer

Sample without an oxide layer

Fig 4-6 Comparison between grain growths at equivalent points in the two samples for scanning velocity of 5μm/s.

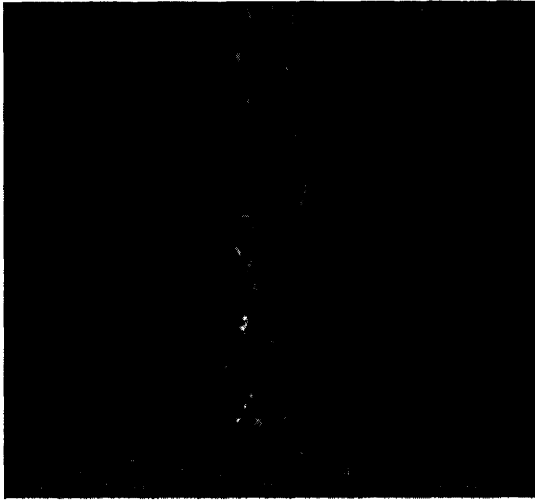

Sample with an oxide layer

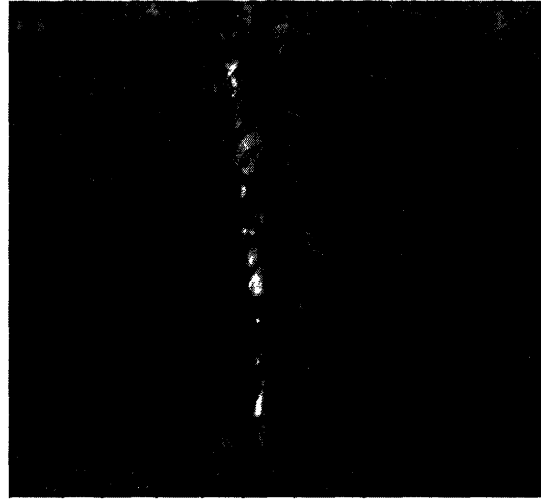

Sample without an oxide layer

(a) Low magnification Image 10KX

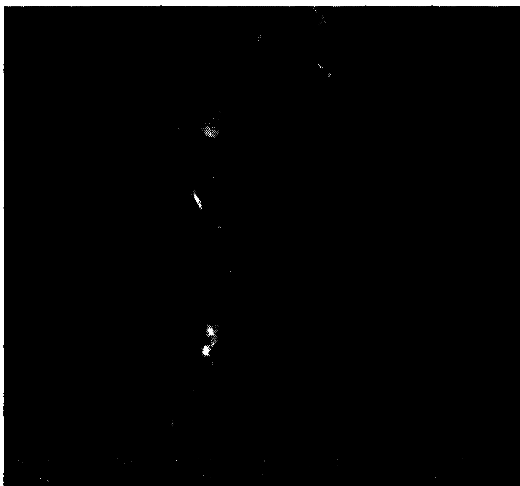

Sample with an oxide layer

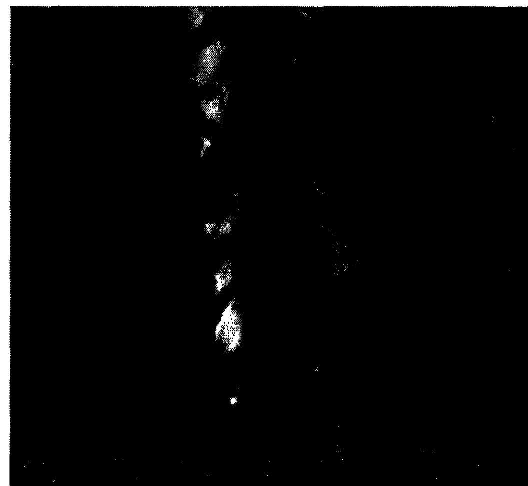

Sample without an oxide layer

(b) High magnification Image 20KX

Fig 4-7(a) and(b) Comparison between grain growths at equivalent points in the two samples for scanning velocity of 60μm/s.

The average grain length in the scanning direction and in the direction perpendicular to the scanning direction were compared for the three conditions and the they are plotted on Figs 4-8, 4-9. The average ratio of the grain length in the two directions was also compared and is plotted on Fig 4-10.

The average grain length in the scanning direction is found to be higher in the sample without an oxide layer. The average grain sizes in the direction perpendicular to the scanning direction were found to be comparable. The average of the ratio of the grain size in the direction of scanning to the grain size in the direction perpendicular to the scanning direction was found to be higher for the sample without an oxide layer.

This can explained by the higher thermal gradients in the scanning direction which lead to less grain growth ahead of the beam and thus the grain boundaries are pushed more effectively in the direction of scanning leading to large grains as described in the introductory chapter (chapter 1). The thermal gradients associated with the three conditions are plotted in Fig 4-10, 4-11.

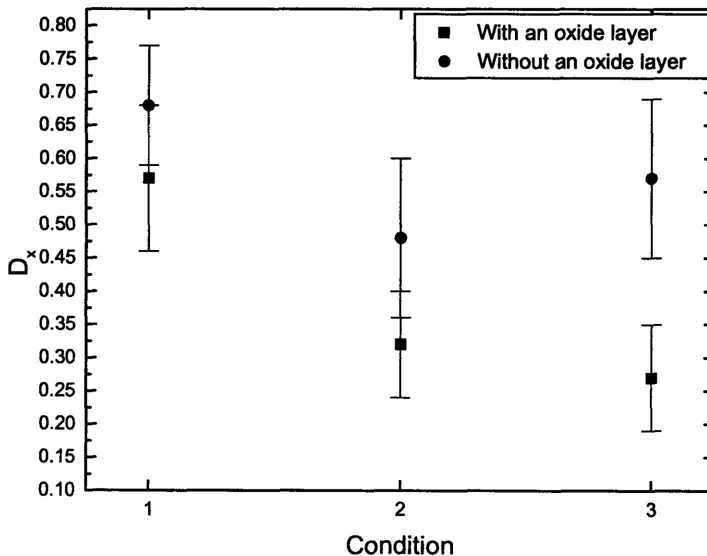

Fig 4-8 Average grain size in the scanning direction under the three conditions.

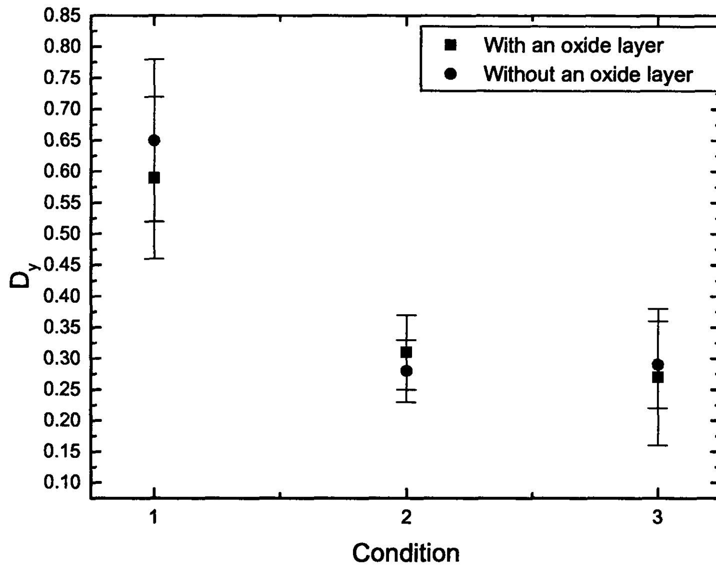

Fig 4-9 Average grain size in the direction perpendicular to the scanning direction under the three conditions.

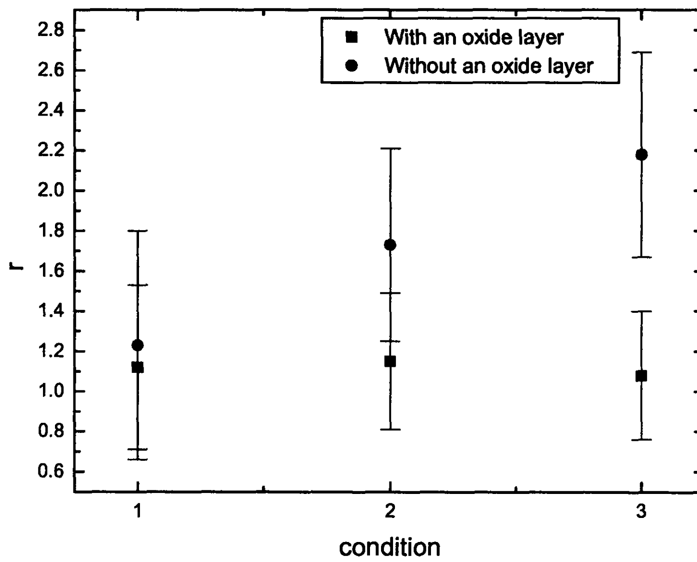

Fig 4-10 Average ratio of the grain length in the scanning direction to the grain length in the perpendicular direction.

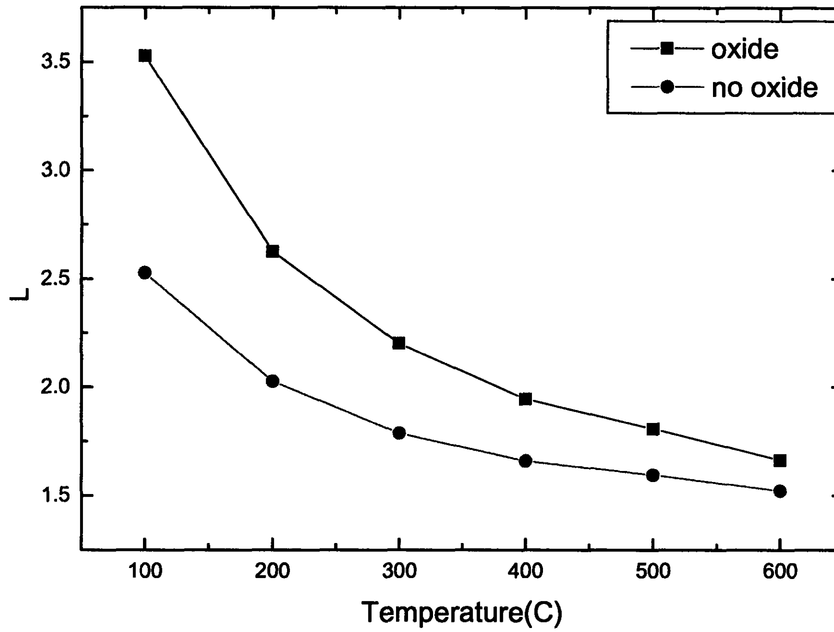

Fig 4-11 Thermal gradients in the scanning direction for condition1 and 2, L is defined such that the thermal profile along the scanning direction(x axis) fits the equation

$$T = T_0 + (T_{max} - T_0)\exp\left(\frac{-(x - x_0)}{L}\right)$$

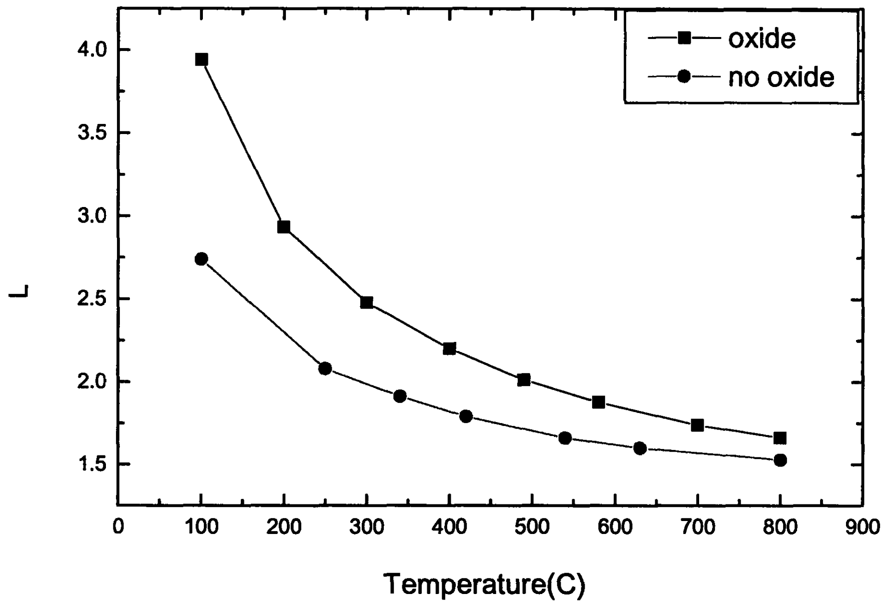

Fig 4-12 Thermal gradients in the scanning direction for condition 3, L is defined such that the thermal profile along the scanning direction(x axis) fits the equation

$$T = T_0 + (T_{\max} - T_0)\exp\left(\frac{-(x - x_0)}{L}\right)$$

The higher average grain sizes in the scanning directions (Fig4-8) in the sample with no oxide layer can be explained by the steeper thermal gradients (Fig 4-11 and 4-12). The grains are not as large as predicted by the simulations done by Hau-Riege(Fig 1-6, Hau01) which predict bamboo grains size of the order of 10μm for L<2. However, the simulations were done for different conditions and for patterned lines. The larger difference in the average grain length in the scanning direction for the condition 3 is expected because of the higher ratio of the thermal gradients in that condition (Fig 4-12).

Chapter 5

Summary and Future work

5.1 Summary

Various microstructure regimes resulting from scanned ns-pulse laser annealing of Cu thin films were investigated:

a) Ablation
b) Agglomeration
c) Grain Growth.

Ablation was observed at higher powers. Below the threshold power for ablation, agglomerated structures were observed over a range of powers. At even lower powers grain growth was observed. The ranges of power in which these regimes were observed shifted towards higher power as the scanning velocities were increased. These regimes also shifted towards lower power for the samples with a silicon dioxide layer under the Cu film.

Ablation thresholds for the two kinds of samples were compared with respect to thermal modeling. For each velocity, the maximum temperatures attained in samples with and without oxide layers were found to be comparable.

In the agglomeration regime, the structures formed were observed to be quasi-periodic. For both kinds of samples, the period of these structures decreased as the scanning velocity decreased and the power increased.

The grain growth regime was observed at powers below those that led to agglomeration. The average grain size was found to increase as the scanning velocity was decreased and

as the power was increased. A comparison of the thermal doses at the power at which grain growth initiated was done using FEM Thermal Modeling and Matlab simulation. The ratio of thermal doses was found to be comparable.

A comparison of a sample with an oxide layer and a sample without an oxide layer underneath the Cu film was carried out, to study the effect of thermal gradients on grain growth caused by scanned laser annealing. Using thermal modeling and a Matlab simulation to estimate the thermal dose, a scheme was devised to scale powers and pulsing frequency to get equivalent points in the two samples. A comparison of grain growth at equivalent points (maximum temperatures and time) revealed that the average grain size in the scanning direction was larger in the sample without any oxide layer. This can be explained by the steeper thermal gradients in these samples.

5.3 Future work

Identification of the different microstructural regimes and their correlation with laser power and scan velocity are fundamental results which can provide starting points for further work on scanned laser annealing of metallic thin films using pulsed lasers.

Agglomeration was found to lead to formation of quasi-periodic structures in scanned laser annealing of continuous films. Similar experiments on patterned films and lines could be tried to study if more regular structures were formed and the mechanism could explored in more detail. This could have potential applications into making ordered metallic particles.

The average grain size was found to increase with increasing thermal gradient. The thermal gradient could be made steeper by having active cooling of the substrate. Experiments with active cooling could be tried to check if extremely large grained structures were formed. This could then be implemented for Cu interconnects to prepare test structures which could be used to study the role of crystallographic orientation on

interfacial electromigration and the effect of grain boundary scattering on the resistivity of Cu lines.

Bibliography

Bec48 P.A.Beck., M.L.Holtzworth, P.R. Sperry, 1948. *Trans. Am. Inst. Min. (Metall) Eng. 180:163*

Dar85 James M. Darchuk and Leonard R. Migliore 1985, *Lasers & Applications.*

Doh87 R.D. Doherty, D.J. Srolovitz, R.D. Rollett, M.P. Anderson, 1987. *Scripta Metall. 21:675*

Gow99 M.C. Gower,1999 *SPIE 4559:2551*

Hau99 C. S. Hau-Riege and C. V. Thompson , 1999 *Appl. Phys. Lett. 75:1464*

Hau00 C. S. Hau-Riege and C. V. Thompson, 2000 *Appl. Phys. Lett. 77:352*

Hau01 C.S.Hau-Riege, 2001 *Ph.D. Thesis, Department of Materials Science and Engineering, Massachusetts Institute of Technology.*

Hil00 Paul Hilton 2000, *http://www.twi.co.uk/j32k/protected/band_3/kspah004.html* Accessed January 2004.

Hol91 E.A.Holm, N.Zachaaropoulos, and D.J. Srolovitz, and G.S. Grest,1991 *Phy. Rev. A 43:2662*

Hol98 E.A.Holm, N.Zachaaropoulos, and D.J. Srolovitz, 1998 *Acta Matter. 46:3*

Iti04 T. E. Itina , J. Hermann , P. Delaporte and M. Sentis 2004 *Thin Solid Films, 453-454:513-517*

Lom84 L.A. Lompre, J.M. Liu, H. Kurtz and N. Bloembergen,1984 *Appl. Phys. Lett., 44:3*

May70 A.F. Mayadas and M. Shatzkes 1970, *Phys. Rev. B 1: 1382*

Maz94 Mazumder , 1994 *Journal of Laser Applications 16 (2): 65*

Mull87 W.W. Mullins, 1987, *Acta Metall 35:887*

Nar93 J.Narayan, W.L. Brown and R.A. Lemons (eds.), 1993, *Solid Interactions and Transient Thermal Processing of Materials, Elsevier, New York.*

Ohr92 M.Ohring,1992 Th*e Materials Science of Thin Films 594*

Pla87 J.E. Plamre, C.V. Thompson, H.I. Smith 1987. *J.Appl. Phys., 62:2492*

Ras96 R.L. Rasera and J.B. Bernstein, 1996 *IEEE Trans. on Comp., Pack. And Manuf. Tech., Part A, 19:554-561*

Rum96 P.T. Rumsby, E.C.Harvey, D.W. Thomas 1996 , *SPIE 2921, 684*

She96 Y.L. Shen, S. Suresh, and J.B. Bernstein, 1996 *IEEE Trans. on Elect. Dev., 43: 402-410*

Ste02 Werner Steinho¨gl, Gu¨nther Schindler, Gernot Steinlesberger, and Manfred Engelhardt 2002, *Phys. Rev. B 66, 075414*

Tho90 C.V. Thompson 1990, *Annu. Rev. Mater. Sci. 20:245-68*

Urb02 S. Urban, F. Falk, T. Gorelik, U. Kaiser, *Materials Science Forum 2002, 389-393: 871-874*

Ven04 J. Venturini ,M. Hernandez ,G. Kerrien , et al.2004 *Thin Solid Films 453-54: 145-149*

Wei02 V. Weihnacht and W. Brückner 2002, *Thin Solid Films, 418, Issue 2, 136-144*

Yog03 Yusuke Yogoro, Atsushi Masuda and Hideki Matsumura 2003 *Thin Solid Films, 430, Issues 1-2, 296-299*

Room 14-0551
77 Massachusetts Avenue
Cambridge, MA 02139
Ph: 617.253.5668 Fax: 617.253.1690
Email: docs@mit.edu
http://libraries.mit.edu/docs

DISCLAIMER OF QUALITY

Due to the condition of the original material, there are unavoidable flaws in this reproduction. We have made every effort possible to provide you with the best copy available. If you are dissatisfied with this product and find it unusable, please contact Document Services as soon as possible.

Thank you.

Some pages in the original document contain pictures, graphics, or text that is illegible.